

Simple Photoelectric Absorption during Dipping in the ASCA Observation of XB 1916-053

M. J. CHURCH^{1,2}, T. DOTANI², M. BALUCIŃSKA-CHURCH^{1,2}, K. MITSUDA²,
T. TAKAHASHI², H. INOUE² AND K. YOSHIDA³

ABSTRACT

We report results of analysis of the ASCA observation of the Low Mass X-ray Binary dipping source XB 1916-053 made on 1993, May 2nd, during which dipping was very deep such that in the deepest parts of dips, the X-ray intensity in the band 0.5 - 12.0 keV fell to zero, demonstrating that all emission components were completely removed. The best-fit orbital period of the binary system determined from the X-ray data was found to be 3005 ± 10 s. The high quality ASCA data allowed spectral evolution in dipping to be systematically investigated by spectral analysis in intensity bands covering the full range of dipping from intensities close to zero to non-dip values. We have shown that the spectra can be well fitted by the same two-component model previously used to give good explanations of the very different dip sources X 1755-338 and X 1624-490, consisting of point-source blackbody emission from the neutron star plus extended Comptonised emission probably from the accretion disk corona. In the case of XB 1916-053 we show that all levels of dipping can be fitted using $kT_{\text{bb}} = 2.14 \pm 0.28$ keV and power law photon index $= 2.42 \pm 0.21$ which are the best-fit values for non-dip data, together with the corresponding non-dip normalisations. Dipping is shown to be due to large increases of column density for the point-like blackbody, combined with the extended power law component being progressively covered by absorber until in the deepest parts of dips, the partial covering fraction approaches unity. This approach differs radically from the “absorbed plus unabsorbed” approach previously used in spectral modelling of XB 1916-053 and similar sources, in which the normalisation of the unabsorbed component is allowed to decrease markedly in dipping, behavior generally attributed to the effects of electron scattering. Thus we have shown that spectral evolution in XB 1916-053 can be explained simply in terms of photoelectric absorption without the need for substantial electron scattering. This explanation is supported by calculation of the relative importance of photoelectric absorption and electron scattering in the absorbing region which shows that little electron scattering is expected in the ASCA energy band.

Subject headings: accretion, accretion disks — scattering — (stars:) binaries: close — stars: circumstellar matter — stars: individual (XB 1916-053) — X-rays: stars

¹School of Physics and Space Research, University of Birmingham, Edgbaston, Birmingham B15 2TT, UK

²Institute of Space and Astronautical Science, Yoshinodai 3-1-1, Sagami-hara, Kanagawa 229, JAPAN

³Faculty of Engineering, Kanagawa University, 3-27-1 Rokkakubashi, Kanagawa-ku, Yokohama 221, JAPAN

1. Introduction

XB 1916-053 is an important member of the class of ~ 10 Low Mass X-ray Binary (LMXB) sources that exhibit decreases in X-ray intensity at the orbital period, generally accepted as being due to absorption in the bulge in the outer accretion disk where the flow from the companion impacts on the outer disk (White and Swank, 1982). XB 1916-053 is unusual in several respects: it has the shortest orbital period of the dipping sources, 50 min (Walter et al. 1982). It has a depth of dipping that is highly variable which at times reaches 100%. The source is also notable because of the difference between the X-ray period and the optical period of $\sim 1\%$ (Grindlay et al. 1988).

Three Exosat observations were made and the results of Smale et al. (1988) showed that the average extent of dipping changed markedly between the observations as shown by comparing the light curves folded on the X-ray period for the 3 observations. Spectral analysis showed that non-dip data for all 3 observations was best-fitted by a simple power law model with photon index Γ close to 1.80. Dip spectra were selected in intensity bands from all 3 observations, for which the best fit was a model consisting of two power laws, each with the index fixed at the above value. The column density of the one component could be held at the quiescent value, while that of the other component increased strongly in dipping; ie there was an absorbed and an unabsorbed term. For the unabsorbed component, the normalisation decreased strongly in dipping. This “absorbed plus unabsorbed” approach has been used for several of the dip sources. It has been applied to the sources: XBT 0748-676 (Parmar et al. 1986), X 1254-690 (Courvoisier et al. 1986) and X 1624-490 (Jones and Watson, 1989). It is clear that the parameters of the source emitting regions cannot change coincidentally with dipping and the strong decrease in normalisation of the unabsorbed component has been attributed to the effects of electron scattering in the absorber (Parmar et al 1986; Smale et al. 1988); ie there is a decrease in flux from the source due to scattering which does not reveal itself as low energy absorption. More recently, GINGA data on XB 1916-053 has also been fitted by the absorbed plus unabsorbed approach (Smale et al. 1992; Yoshida et al., 1995). Yoshida et al. showed that the variation in normalisation can be reproduced as absorption by cold matter if electron scattering in the absorber is taken into account.

XB 1916-053 shows increases in hardness during dip ingress. It was originally expected that all of the dipping sources should show hardening during dipping, due to photoelectric absorption of the X-ray spectrum in the absorbing bulge which preferentially removes the lower energy X-rays. However, the dip sources do not in general follow this expectation; some sources show a hardening, but some show a marked softening in dipping, eg X 1624-490 (Church and Balucinska-Church, 1995) which is totally unexpected on simple physical models, ie with a single emission component. Furthermore X 1755-338 has dipping which is independent of energy in the band 1 - 10 keV (White et al. 1984).

Several types of spectral model have been used in fitting the dipping sources. The Exosat spectra of several dipping sources were fitted by a Comptonisation model (White et al. 1988) represented by a single component absorbed cut-off power law. Other workers have used two-component models, notably Mitsuda and co-workers (see for example, Mitsuda et al. 1984). Apart from this difference in approach, individual dipping sources have generally been fitted by different spectral models. In particular, the absorbed plus unabsorbed approach has involved different spectral forms when applied to different sources; ie power law plus power law, cut-off power law plus cut-off power law, etc. More recently, Church and Balucinska-Church (1993, 1995) have proposed a two-component or “complex continuum” model which has been able to explain the softening in dipping in X 1624-490 and the energy-independence of dipping in X 1755-338 using the same model. In this model, X-ray emission originates as blackbody radiation from the boundary layer at the surface of the neutron star, plus power law emission representing Comptonisation in an accretion disk corona (valid at energies much lower than the Comptonisation break). In the above sources, the model shows that dipping is primarily due to absorption of the point-source blackbody emission with comparatively little absorption of the extended power law emission. Whether there is softening, hardening or energy-independence depends mostly on the blackbody temperature. In X 1624-490, this is higher than in X 1755-338 ($kT_{\text{bb}} = 1.39$ keV compared with 0.88 keV), so that removal of the blackbody leaves the residual spectrum softer than in non-dip emission.

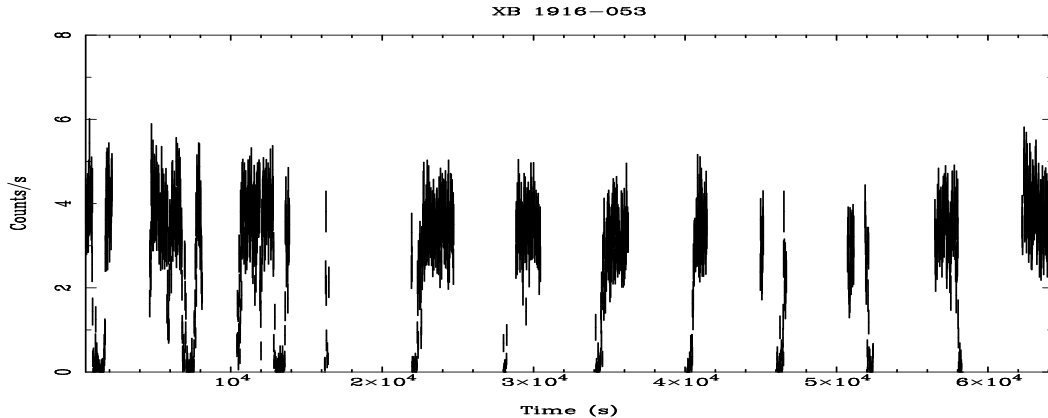


Fig. 1.— ASCA GIS2 light curve for the complete 18 hr observation in the energy band 0.5 - 12.0 keV with 16 s binning.

The main aim of the present work was to test the complex continuum model in the case of XB 1916-053 using high quality ASCA data, and to test whether this physical model can offer an alternative to the absorbed plus unabsorbed approach.

2. Results

The 18 hr observation of XB 1916-053 was made on 1993, May 2nd. with the satellite ASCA (Tanaka et al. 1994). The quality of the data was very good, and we present here results primarily for analysis of the GIS2 and GIS3 detector data (see Ohashi et al. 1996). The data were screened to remove regions of South Atlantic Anomaly passage, to restrict elevation of the source above the limb of the Earth to more than 5° , particle cut-off rigidity to more than 6, angular deviations of the telescope pointing to less than 0.6 arcmin, and the radiation belt parameter to less than 500. Rise-time discrimination was applied to remove detector particle background. Data were pre-selected from the image to remove the region of the calibration source and outer ring in the image, and source data were taken from a 6 arcmin radius circle centered on the source. Various tests were made on the best way of subtracting background, and eventually we found that the most reliable background subtraction could be obtained by taking background data from a circular region of radius 8 arcmin offset from the center of the image by the same amount as the source region (about 2 arcmin) diametrically opposite to the source containing no visible point sources. This region pro-

vided a sufficiently large count for background subtraction which is important, with a count rate of 0.13 c/s.

The total observation of XB 1916-053 spanned about 22 orbital cycles. The good data inbetween SAA passage and Earth occultation included parts of about 10 dips. Much of this dip data was very fragmented; however during the first 5 orbital cycles observed, complete data were obtained for 2 orbital cycles. In addition complete data were obtained from this part of the observation for one more dip. Burst data were contained in the observation, but did not remain in GIS data after screening and so did not affect our spectral analysis.

2.1. Light Curves and Hardness Ratio

Light curves were extracted in various energy bands and it was found that during part of every dip, the count rate fell to zero in the total band of the GIS detectors 0.5 - 12.0 keV. The background-subtracted light curve of the GIS2 data is shown in Fig. 1, from which the good coverage of 3 dips in the early part of the observation can be seen, and the relatively poor definition of later dips. Interdips between the main dips can also be seen.

Hardness ratio was obtained by dividing the c/s in the band 2.0 - 12.0 keV by the c/s in the band 0.5 - 2.0 keV, and the light curves in these bands and the plot of hardness ratio against time are shown in Fig. 2 for one orbital cycle including non-dip, inter-

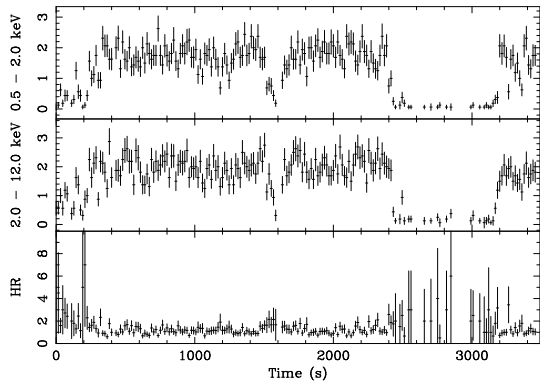


Fig. 2.— GIS2 light curves for the 3rd section of data in Fig. 1 in the energy bands 2.0 - 12.0 keV and 0.5 - 2.0 keV and the hardness ratio formed by dividing these.

dip and dip data. Increases in hardness ratio at dip ingress and egress and in interdips can be seen; during deep dipping when all count rates were very small the hardness ratio is not well-determined. The depth of dipping defined as the maximum percentage decrease in count rate was investigated as a function of energy by plotting light curves in several energy bands. In the lower bands 0.5 - 2.0 keV, 2.0 - 4.0 keV and 4.0 - 6.0 keV, dipping was 100%; in the higher band 6.0 - 12.0 keV, the depth possibly decreased to $95 \pm 5\%$. Thus dipping was remarkably deep at all energies implying an absorber of high column density completely covering all emission regions. In the interdips dipping was not 100%.

2.2. Light Curves Folding Analysis

For determining the best-fit X-ray orbital period, we used fast mode SIS0 data for the whole observation with time resolution of 1 s. The data were folded on trial periods spanning the range 2900 s to 3100 s to find the most probable period, from which a best value of 3005 ± 10 s was obtained. In Fig. 3 we show the GIS2 light curve from the first 5 orbital periods in the observation folded on this period (to avoid severe distortion of the folded light curve by adding in data not containing interdips, for example). It is difficult to be certain of the errors attached to this period. The errors of ± 10 s represent the range of possible periods around the most likely value in the plot of

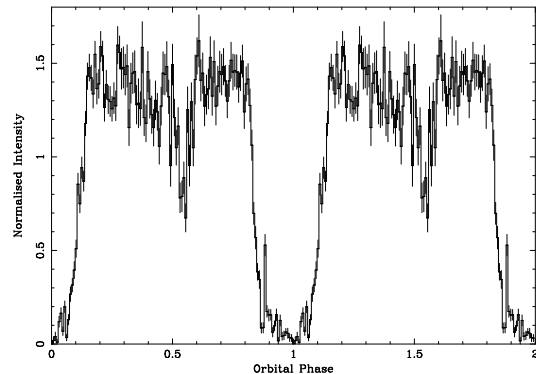


Fig. 3.— ASCA GIS2 data folded on the 3005 s best-fit orbital period.

χ^2 versus period produced by the period searching program, consistent with the scatter of the χ^2 points. However, the period is being determined using dip data of variable length, depth and quality, and the errors are inevitably larger than in fitting, for example, a coherent oscillation. By folding the data on periods outside the range of the errors above (within 3005 ± 20 s) it was found that folded light curves having shapes consistent with the raw light curves could be produced, so that the real errors may be somewhat larger than those quoted. Previous values for the X-ray period were determined, for example, from *Exosat* data to be 3015 ± 17 s, and from GINGA data to be 3005 ± 6.6 s (Smale et al. 1992). From Fig. 3, it can be seen that the main dip lasts 33% of the orbital cycle implying an absorbing region that subtends an angle of 120° at the neutron star. The consequence of this is that the absorbing region must be very extended azimuthally and may therefore also be extended in height above the disk. Thus it might be expected that the depth of dipping can reach 100% as observed, since all emission regions can be covered by the absorber during dips, ie not just point source emission from the neutron star, but also extended emission regions. This will be relevant to the spectral modelling discussed below.

2.3. Spectral Evolution in Dipping

The very large depth of dipping in XB1916-053 during the ASCA observation, the complete coverage of several dips and the high quality of the data, have

allowed detailed investigation of spectral evolution in dipping by dividing the data into intensity bins. GIS2 data were divided into bands corresponding to non-dip data: 4.0 - 5.0 c/s and various levels of dipping at 3.0 - 4.0 c/s, 2.0 - 3.0 c/s, 1.0 - 2.0 c/s and 0.0 - 1.0 c/s and spectra produced. The corresponding GIS3 data were selected by using the time filters produced when GIS2 data were selected into intensity bands. Because of differences between the detectors, this GIS3 data formed bands somewhat different in intensity from the original GIS2 bands. GIS2 and GIS3 spectra were added, systematic errors of 2% added to each channel and the data regrouped to a minimum of 100 counts per bin. Channels below 0.7 keV and above 10.0 keV were ignored. Response functions and effective areas were used in the spectral fitting as appropriate to the regions from which the data were extracted, and the GIS2 and GIS3 effective area files combined. Background spectra from GIS2 and GIS3 were combined appropriately. Non-dip and dip data were fitted by a number of spectral models, beginning with various simple models such as an absorbed power law, absorbed blackbody and absorbed bremsstrahlung. The absorbed power law model gave a formally acceptable fit to all intensity bands except the lowest intensity band for which the reduced χ_r^2 was 2.8; however the power law photon index varied between 1.76 in non-dip and 0.61 in deep dipping which is clearly not acceptable physically. The absorbed blackbody could not fit non-dip data with a χ_r^2 of 9.9, and the absorbed bremsstrahlung model had χ_r^2 values in the range 1 - 4.7 for various intensity bands and kT values varying between 9.4 and 200 keV. Thus it is clear that simple models cannot be used. Consequently, we next attempted to fit the kind of two-component model used for the sources X 1755-33 and X 1624-490 (Church & Balucinska-Church 1993, 1995), consisting of a blackbody component associated with the neutron star and a power law component associated probably with the accretion disk corona. Each component was given its own absorption term and the model may be represented as: $AB_1 * BB + AB_2 * PL$. The two sources above could be fitted well by this model with kT_{bb} and Γ and the normalisations of the 2 components fixed at the non-dip values; dipping was due primarily to increases of column density for the blackbody. In the case of XB 1916-053, the dip data could not be fitted with the normalisations held constant, with χ_r^2 values for deep dip data as large as 19.3. This was related to the appearance of a double-humped shape

to the dip spectra, ie the apparent existence of an unabsorbed component at lower energies, or soft excess. In the absorbed plus unabsorbed approach, the low energy hump is the unabsorbed component which persists into dipping even though the higher energy hump is strongly absorbed. As we were unable to fit the two-component model with normalisations fixed at the non-dip values, we next fitted the same model with free normalisations. This model gave an acceptable fit to all intensity levels. The normalisation of the power law component decreased by a large factor and the blackbody column density increased by a large amount in dipping. Thus this is a form of the absorbed plus unabsorbed approach which represents a halfway stage between the normal absorbed and unabsorbed approach and our final best-fit modelling below.

It is an integral part of the complex continuum model that the source emission parameters cannot change during dipping, and so the normalisations should be held constant. However during dipping the count rate falls to zero, and the model must reproduce this. Thus in this particular source the appropriate form of the complex continuum model to use must allow for all emission regions to be covered by the absorber, and so we applied the model in the following form: $AB_1 * BB + AG * [AB_2 * f + (1-f)] * PL$ where AG represents Galactic absorption and f is a partial covering fraction. The blackbody absorption term, of course, also includes Galactic absorption; however we have investigated the best values of column density of the two components as discussed below, and this was done by varying the AG term. With the above spectral model, a good fit was obtained to the non-dip data giving values for the blackbody temperature $kT_{bb} = 2.14 \pm 0.28$ and power law index $\Gamma = 2.42 \pm 0.21$. With kT_{bb} and Γ and the corresponding normalisations held fixed at the best-fit non-dip values, very good fits could be obtained to all intensity levels of dip data, with χ_r^2 always less than 0.84. Extensive testing was carried out to determine whether interdips should be included with main dip data. It was found that differences in spectral fitting parameters between dip data and interdip data at the same intensity were generally within 90% confidence errors, although there was some tendency for blackbody column densities to be higher in dips. To obtain better statistics, the final analysis was carried out including all dips and interdips. The best N_H values for the blackbody and power law components for the non-dip

spectrum were determined by fixing the AG term in the spectral model at various values, and determining χ_r^2 and the total column density of each component.

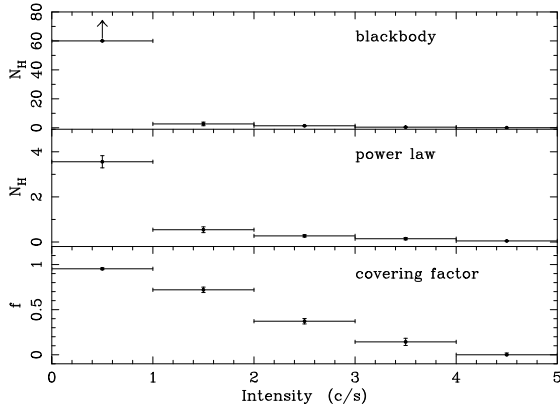


Fig. 4.— Best-fit spectral fitting results : variation of blackbody column density, power law column density and power law partial covering fraction f with intensity. N_H is in units of 10^{23} H atom cm^{-2} .

When the AG term was fixed at $2 \cdot 10^{21}$ H atom cm^{-2} (the Stark et al. (1992) value), the blackbody column density became very large at $60 \cdot 10^{21}$ H atom cm^{-2} with χ_r^2 equal to 9.0. As the AG term was increased, χ_r^2 decreased to a value of ~ 0.78 when the blackbody and power law column densities were equal with a value of $4.75 \cdot 10^{21}$ H atom cm^{-2} . This value is in excess of the Stark et al. value implying a degree of intrinsic absorption in the source during this observation. Plots of the spectral fitting results as a function of X-ray intensity are shown in Fig. 4, and parameter values are given in Table 1.

Fig. 5 shows source spectra for non-dip, intermediate dip and deep dip data, together with the 2 model components, to illustrate how the spectral components of the complex continuum model can successfully model

Table 1: Best fit spectral fitting results.

I ^a	$N_H(\text{BB})^b$	$N_H(\text{PL})^b$	f	χ_r^2
4 - 5	0.48 ± 0.18	0.48 ± 0.18	$0.00^{+0.02}_{-0.0}$	0.78
3 - 4	4.3 ± 0.6	1.5 ± 0.5	0.14 ± 0.04	0.84
2 - 3	13.8 ± 2.7	2.7 ± 0.5	0.37 ± 0.03	0.84
1 - 2	26.7 ± 12.6	5.4 ± 1.3	0.72 ± 0.03	0.67
0 - 1	>600	35.6 ± 2.7	0.95 ± 0.01	0.49

^a intensity in c/s; ^b in units of 10^{22} H atom cm^{-2}

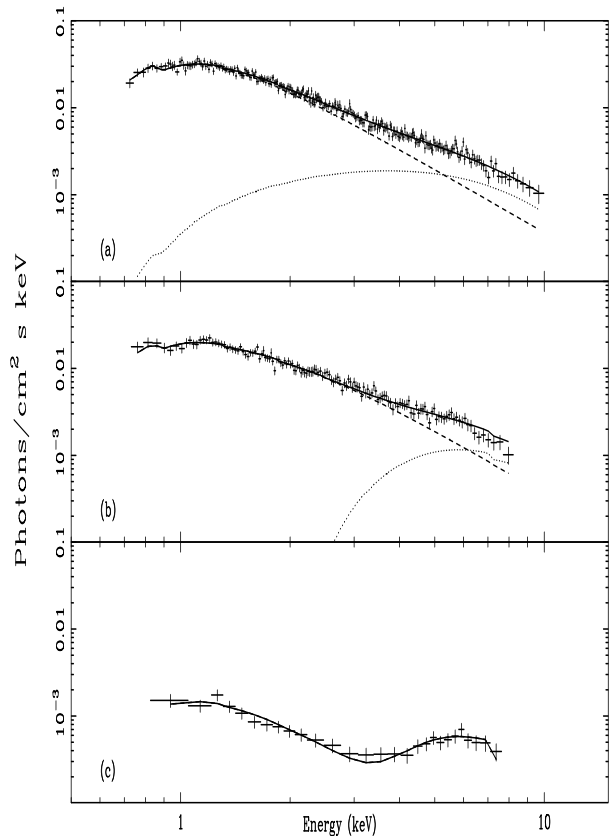


Fig. 5.— Contributions of the blackbody (dots) and the power law (dashes) to the net photon spectrum for (a) the non-dip spectrum, (b) the intensity band 2.0 - 3.0 c/s and (c) the intensity band 0.0 - 1.0 c/s. Note that in (c) the blackbody is totally absorbed.

the dipping. It can be seen that there is little evidence for spectral line features in the non-dip data. Because of its relatively high temperature ($kT_{\text{bb}} = 2.14$ keV), the blackbody peaks at ~ 6.5 keV, ie in the higher energy part of the ASCA spectrum. As this component is point-like it is immediately covered by absorber and N_H increases by about a factor of 25 as the intensity falls from 4.0 - 5.0 c/s to 2.0 - 3.0 c/s. The power law, however, starts with a partial covering fraction of zero and at first suffers little absorption. Thus, as dipping develops, the power law remains as a low energy peak while at higher energies the blackbody is strongly absorbed. In deeper dipping, N_H for the blackbody increases to at least $6000 \cdot 10^{21}$ H atom cm^{-2} , completely removing this component. The par-

tial covering fraction reaches 0.95, N_{H} for the power law also becomes high at $350 \cdot 10^{21}$ H atom cm^{-2} , and the power law is split between the low energy hump which is the 5% not covered, and the higher energy hump which is covered, but not totally absorbed. Finally, the fluxes of both components become zero. Thus there are no changes in normalisation, and the dipping can be explained simply in terms of photoelectric absorption of the point source blackbody emission from the neutron star combined with absorption of the extended power law component by a relatively large absorbing bulge such that the extended component is progressively covered by the absorber. In this model, the “absorbed” part is the blackbody plus the covered part of the power law, and the “unabsorbed” part is the uncovered power law.

3. Discussion

We have demonstrated that the two-component model can give a good description of spectral evolution in XB 1916-053. In this model, emission originates as point-source blackbody emission from the neutron star plus extended power law emission probably from the accretion disk corona. In the case of XB 1916-053, the source intensity in the band 1.0 - 10.0 keV often actually becomes zero in the deepest parts of dips. In X 1755-338 and X 1624-490, dipping was not 100% and spectral evolution during dips was explained by the 2-component model with dipping being primarily due to absorption of the blackbody (Church and Balucinska-Church 1993, 1995). In the case of XB 1916-053, it was necessary to allow the spectral modelling to take account of the fact that the power law component must be totally removed in deepest dipping. The modelling we performed showed that it was not sufficient to use a spectral form $\text{AB} \cdot \text{BB} + \text{AB} \cdot \text{PL}$; the data could not be fitted by this model with normalisations fixed. It was necessary to allow the extended power law component in our model to be progressively covered by the absorber; extended emission would not be covered essentially instantaneously as is the point-source component. With the inclusion of the partial covering term, the two-component model provides very good fits to the spectra.

The fluxes of the blackbody and power law components in the non-dip data in the energy range 1 - 10 keV are $0.98 \cdot 10^{-10}$ erg cm^{-2} s^{-1} and $1.83 \cdot 10^{-10}$

erg cm^{-2} s^{-1} respectively, so that the blackbody contributes 34% to the total energy flux in this band. In X 1755-338 and X 1624-490, in which the two-component model showed that dipping was due primarily to absorption of the blackbody, the spectral evolution in dipping is determined by kT_{bb} ; in X 1624-490 kT_{bb} was 1.39 keV, the blackbody peaking at ~ 4.5 keV, ie it was relatively hard such that the residual power law spectrum when the blackbody was absorbed was softer. XB 1916-053 has even higher kT_{bb} of 2.14 keV; however this does not determine the spectral evolution during dips since both components are absorbed. The low energy cut-off of the spectrum is determined by the power law component, and the hardening observed at dip ingress is clearly simply due to absorption of the low energy part of the spectrum.

Perhaps the most interesting question is whether we expect electron scattering to be important in the absorbing region producing the dips. In other dip sources in which the absorbed plus unabsorbed approach was not used, electron scattering was not thought to be important. Electron scattering may take place in XB 1916-053 between the source regions and the absorbing bulge in the outer disk, but this will occur in both non-dip and dip cases and so is not relevant. In the absorbing region, we can determine the state of ionization by estimating the ionization parameter ξ as follows, using the column density of the point source blackbody component as a probe of density along a track through the absorbing bulge as dipping develops. As dipping develops, parts of the absorber at different radial positions from the center of the absorber will contribute to attenuation of the incident radiation, having different lengths along the line of sight. We can write $\xi = L\epsilon/N_{\text{H}}r$ where L is the luminosity, r is radial distance from the source and the thickness of the absorber along the line of sight is a fraction ϵ of the accretion disk radius, assumed to fill approximately the Roche lobe of the neutron star. From our best-fit modelling, the unabsorbed flux of the source in the band 1 - 20 keV is $4.1 \cdot 10^{-10}$ erg cm^{-2} s^{-1} , and the corresponding luminosity is $3.4 \cdot 10^{36}$ erg s^{-1} , using a distance of 8.4 kpc (Smale et al. 1988). As dipping commences, in the intensity band 3.0 - 4.0 c/s, the blackbody has column density $4.3 \cdot 10^{22}$ H atom cm^{-2} and estimating ϵ as 0.03, we find that $\xi = 70$ erg $\text{cm} \text{s}^{-1}$. For this value, ionization will not be complete. In deepest dipping, N_{H} rises to at least $6 \cdot 10^{24}$ H atom cm^{-2} , and the thickness of absorber along the line of sight

will be maximum, so if we take $\epsilon \sim 0.3$ we get $\xi = 5$, such that some elements only can be, at most, singly ionized.

In both cases described above where ionization is not complete, the relative importance of photoelectric absorption and electron scattering is given by the ratio $N_{\text{H}} \cdot \sigma_{\text{PE}} / N_{\text{e}} \cdot \sigma_{\text{T}}$, where σ_{PE} is the total photoelectric absorption cross section, σ_{T} is the Thomson scattering cross section, and N_{e} is the electron column density. This follows from the dependences of the processes on $\exp - (N_{\text{H}}\sigma_{\text{PE}})$ and $\exp - (N_{\text{e}}\sigma_{\text{T}})$.

For a completely ionized plasma of a medium with Solar abundances, it can be calculated that the electron density n_{e} is related to the ion density n_{i} via $n_{\text{e}} \simeq 1.2 \cdot n_{\text{i}}$, since elements other than H contribute more than 1 electron, but with small abundances. Thus in the above cases $N_{\text{H}} \simeq N_{\text{e}}$ and the above ratio is dominated by the ratio of cross sections. At 1 keV, $\sigma_{\text{PE}}/\sigma_{\text{T}} \simeq 500$, at 4 keV, $\sigma_{\text{PE}}/\sigma_{\text{T}} \simeq 10$, and at 10 keV, $\sigma_{\text{PE}}/\sigma_{\text{T}} \simeq 2$. Thus photoelectric absorption strongly dominates over electron scattering throughout most of the ASCA band. We should also consider how this depends on N_{H} . As the column density increases in deep dipping corresponding to the central regions of the absorber, at $N_{\text{H}} = 1.5 \cdot 10^{24}$ H atom cm^{-2} , the optical depth for electron scattering becomes unity. However the product $N_{\text{H}}\sigma_{\text{PE}}$ will be very much greater than 1; ie the probability of photoelectric absorption is still much higher than that of electron scattering. If incident photons are allowed to be simultaneously absorbed and scattered, in deep dipping the factor $\exp(-N_{\text{e}}\sigma_{\text{T}})$ implies that an appreciable fraction of the radiation incident upon the absorber could be scattered. The average column density of $35.6 \cdot 10^{22}$ H atom cm^{-2} from spectral fitting implies a loss of 20% by scattering, and it could be argued that the spectral model we have applied should be modified for deep dipping. However if there is a density gradient in the absorber, with $N_{\text{H}} = 10^{22} - 10^{23}$ H atom cm^{-2} in the outer layers, the optical depth for absorption will be > 1 , but for scattering < 1 . Thus photons will be preferentially removed before they reach the higher density central regions where scattering would play a part. At 10 keV, this preferential absorption will be much weaker, so that in deepest dipping, electron scattering of the high energy photons will take place. The blackbody emission is by this stage of dipping already highly absorbed leaving flux only in the range just below 10 keV. Thus our value of N_{H} for the blackbody in deepest dipping of

$> 600 \cdot 10^{22}$ H atom cm^{-2} may be an overestimate as some decrease of normalisation may be appropriate for this term, which would imply a smaller N_{H} value.

Thus, in summary, we have shown that the physical model used by Church and Balucinska-Church to explain the dipping sources X 1755-338 and X 1624-490 also provides a good explanation for XB 1916-053. In all of these cases, the model can be expressed as point source blackbody emission plus extended Comptonised emission which is modified by partial covering. For the first two sources the partial covering fraction f is small, but for XB 1916-053 f becomes large in dipping. Consequently it is possible to explain the dipping in XB 1916-053 purely in terms of photoelectric absorption in a bulge in the outer accretion disk. There is no need for there to be substantial electron scattering, and we have shown that in the ASCA band little scattering is, in fact, expected. The explanation of 3 very different members of the dipping class by the two-component model makes it increasingly likely that it will be able to explain all members of the class.

REFERENCES

- Church M. J. and Balucinska-Church M., 1993, MNRAS 260, 59.
- Church M. J. and Balucinska-Church M., 1995, A&A 300, 441.
- Courvoisier T. J.-L., Parmar A. N., Peacock A. and Pakull M., 1986, ApJ 309, 265.
- Grindlay J. E., Bailyn C. D., Cohn H., Lugger P. M., Thorstensen J. R. and Wegner G., 1988, ApJ 334, L25.
- Jones M. H. and Watson M. G., 1989, Proc. 23rd ESLAB Symposium on Two Topics in X-ray Astronomy, Eds. Hunt J. and Battrick B., Bologna, Sept. 1989, EAS SP-296.
- Mitsuda K., Inoue H., Koyama K. et al., 1984, PASJ 36, 741.
- Ohashi T., Ebisawa K., Fukazawa Y. et al., 1996, PASJ 48, 157.
- Parmar A. N., White N. E., Giommi P. and Gottwald M., 1986, ApJ 308, 199.
- Smale A. P., Mason K. O., White N. E. and Gottwald M., 1988, MNRAS 232, 647.
- Smale A. P., Mukai K., Williams O. R., Jones M. H. and Corbet R. H. D., 1992, ApJ 400, 330.

- Stark A. A., Gammie C. F., Wilson R. W., Bally J., Linke R. A., Heiles C. and Hurwitz M., 1992, ApJ Suppl 79, 77.
- Tanaka Y., Inoue H. and Holt S. S., 1994, PASJ 46, L37.
- Walter F. M., Bowyer S., Mason K. O., Clarke J. T., Henry J. P., Halpern J. and Grindlay J. E., 1982, ApJ 253, L67.
- White N. E. and Swank J. H., 1982, ApJ 253, L66.
- White N. E., Parmar A. N., Sztajno M., Zimmermann H. U., Mason K. O. and Kahn S., 1984, ApJ 284, L9.
- White N. E., Stella L. and Parmar A. N., 1988, ApJ 324, 363.
- Yoshida K., Inoue H., Mitsuda K., Dotani T. and Makino F., 1995, PASJ 47, 141.